IEEE Photonics Journal
An IEEE Photonics Society Publication

Open Access

Reverse Ridge/Slot Chalcogenide Glass Waveguide With Ultrabroadband Flat and Low Dispersion

Volume 7, Number 5, October 2015

Yanfen Zhai
Chenzhi Yuan
Renduo Qi
Wei Zhang
Yidong Huang

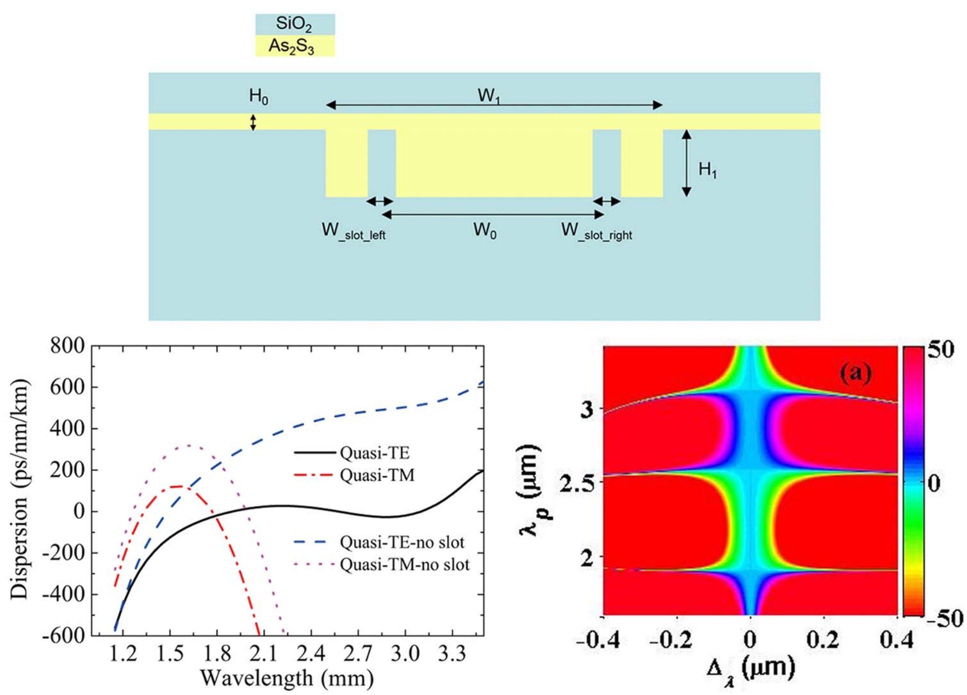

DOI: 10.1109/JPHOT.2015.2456062

IEEE photonics SOCIETY

Reverse Ridge/Slot Chalcogenide Glass Waveguide With Ultrabroadband Flat and Low Dispersion

Yanfen Zhai, Chenzhi Yuan, Renduo Qi, Wei Zhang, and Yidong Huang

Tsinghua National Laboratory for Information Science and Technology, Department of Electronic Engineering, Tsinghua University, Beijing 100084, China

DOI: 10.1109/JPHOT.2015.2456062

Manuscript received May 31, 2015; revised July 7, 2015; accepted July 8, 2015. Date of publication July 23, 2015; date of current version August 24, 2015. This work was supported in part by the 973 Programs of China under Contract 2013CB328700 and Contract 2011CBA00303, by the National Natural Science Foundation of China under Contract 61307068 and Contract 61321004, by Tsinghua University Initiative Scientific Research Program under Contract 20131089382, and by the Basic Research Foundation of Tsinghua National Laboratory for Information Science and Technology (TNList).
Corresponding author: W. Zhang (e-mail: zwei@tsinghua.edu.cn).

Abstract: A reverse ridge/slot hybrid chalcogenide glass (As_2S_3) waveguide with two vertical silicon dioxide slots is proposed in this paper. The fundamental quasi-TE mode of the waveguide shows an ultraflat dispersion with three zero-dispersion wavelengths. Its dispersion is confined between -26 and $+27$ ps/nm/km over a bandwidth of 1370 nm (from 1770 to 3140 nm). Two slots in the waveguide introduce the dispersion tailoring effect on the quasi-TE mode, which provides more flexibility for designing the waveguide dispersion. The nonlinear coefficient and the phase mismatching of the degenerate four-wave mixing (FWM) process in this waveguide are calculated, showing that it can support broadband FWM processes in near- and middle-infrared regions.

Index Terms: Chalcogenide glass waveguides, reverse ridge/slot waveguide, waveguide dispersion, waveguide nonlinearity.

1. Introduction

In recent years, chalcogenide glass waveguides have attracted many attentions as promising candidates to realize on-chip integrated mid-infrared sensing devices [1]–[3] and nonlinear optical devices [4]. As a $\chi^{(3)}$ nonlinear optical material, chalcogenide glass has a high third-order nonlinearity coefficient with negligible two photon absorption (TPA) at telecom bands, resulting in a high Figure of Merit (FOM) [5], [6]. Dispersion design is an important topic for chalcogenide glass waveguides for nonlinear photonic devices, since many nonlinear optical applications, such as soliton formation [7], [8], super-continuum generation [9], [10], four-wave-mixing (FWM)-based parametric amplification, wavelength conversion [11], [12], and comb generation [13], [14], require flat and near-zero dispersion profiles. However, since most chalcogenide glasses used in nonlinear optics have large negative material dispersion at the near-infrared band, the waveguide structure should be designed carefully to obtain a proper waveguide dispersion for compensating the material dispersion [15]–[17]. Traditional ridge and strip structures have been optimized to realize near-zero dispersion at the near-infrared band; however, their bandwidths of near-zero dispersion are limited.

Slots in waveguides can be used to flexibly tailor the waveguide dispersion, which is capable of effectively extending the band of near-zero dispersion [18]–[21]. Zhang [9] proposed a strip/slot hybrid silicon waveguide with a horizontal silicon dioxide (SiO_2) slot. Its dispersion shows a flat profile with four zero-dispersion wavelengths (ZDWs), varying between -22 and 20 ps/nm/km over the bandwidth of 670 nm. Recently, a dual-slot silicon waveguide is proposed, in which the slots are filled with silicon nanocrystals. It has four ZDWs, and its dispersion varies between -24 and 22 ps/nm/km over the bandwidth of 1098 nm [20]. However, these works focused on silicon waveguides, in which high TPA would lead to high nonlinear losses [5]. Recently, a strip/slot hybrid arsenic tri-sulfide (As_2S_3) waveguide with a horizontal SiO_2 slot has been proposed, showing an ultra-flat and low dispersion profile over a wide bandwidth. However, photolithography and lift-off (or dry etching) processes for transferring the waveguide pattern to the As_2S_3 film are required in the fabrication of this structure. More specifically, the (NH_4OH)-based developers used in the photolithography process would attack chalcogenide glass films [18] and impact the quality of the chalcogenide glass waveguides. Hence, the protective coating utilizing thin layers of Polymethylmethacrylate (PMMA), bottom antireflective coating (BARC), or SU-8 (a permanent epoxy negative photoresist) are required to avoid the impact of the alkaline developer on the chalcogenide glass films [22]–[26]. However, this technique complicates the fabrication process of the chalcogenide glass waveguides and may introduce additional loss when removing the protective layer. Recently, the fabrication processes of chalcogenide glass films based on their organic ammonia solution is developing rapidly. However, the residual solvent may lead to the obvious loss when it is used to fabricate optical waveguides in the near-infrared band, since its N-H bonds have an overtone absorption around 1510 nm [27]. Hence, both the requirement on the dispersion property and the feasibility of fabrication should be considered during the design of chalcogenide glass waveguides for integrated nonlinear optical devices.

In this work, we propose a reverse ridge/slot As_2S_3 waveguide, whose fundamental quasi-TE mode has an ultra-flat dispersion profile with three ZDWs. Its dispersion is confined between -26 and 27 ps/nm/km over a bandwidth of 1370 nm (from 1770 nm to 3140 nm). This structure could be fabricated without the photolithography and lift-off processes (or various etching processes) on the chalcogenide glass film, showing great potential for developing nonlinear photonic devices.

2. Waveguide Structure and Its Characteristics

The proposed waveguide is shown in Fig. 1, in which the structure parameters are indicated. First, a groove with two SiO_2 ridges in it could be fabricated in the SiO_2 substrate by the standard E-beam lithography and dry etching process. Then As_2S_3 film could be deposited on the substrate by the thermal evaporation or sputtering. The As_2S_3 film also could be fabricated by the micro-trench filling technique [28] utilizing the solution-processed As_2S_3 glass. Utilizing the low transformation temperature of the As_2S_3 glass, the thermal imprint technique can be used to help the As_2S_3 glass fill the groove to forma flat surface. Finally, a SiO_2 cladding layer would be deposited to protect the As_2S_3 film. As a result, a reverse ridge As_2S_3 waveguide with two SiO_2 slots could be realized. The photolithography, lift-off or various etching processes on the As_2S_3 film could be avoided during the fabrication of the proposed waveguide, which is capable of realizing high-quality chalcogenide glass waveguides.

The dispersion of this waveguide is calculated using the finite element method (FEM). Fig. 2 shows the calculated dispersion of the waveguide with optimized structure parameters ($H_0 = 50$ nm, $H_1 = 600$ nm, $W_0 = 840$ nm, $W_1 = 1190$ nm, $W_{slot\_left} = 90$ nm, $W_{slot\_right} = 84$ nm), which shows broadband width near-zero-dispersion point. To provide a proper dispersion tailoring, the widths of the ridges and the groves nearby should be smaller comparing with the grove depth. Hence, the dry etching process supporting high aspect ratio is required in the fabrication. In the simulation, the material dispersions of SiO_2 and As_2S_3 are calculated according to the Sellmeier equation. The waveguide supports two modes, i.e., the fundamental quasi-TE and

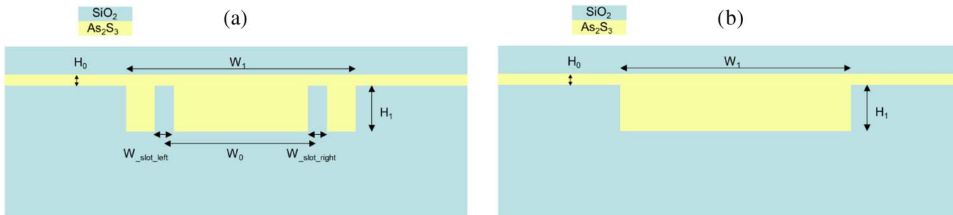

Fig. 1. Structure of the reverse ridge As_2S_3 waveguide. (a) With two SiO_2 slots. (b) Without slots.

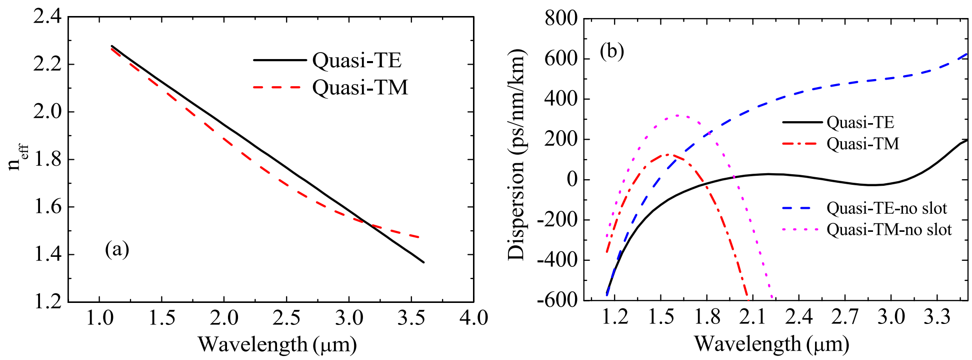

Fig. 2. Effective indices (a) and the dispersions (b) of the fundamental quasi-TE and quasi-TM modes in the proposed waveguide with optimized structure parameters ($H_0 = 50$ nm, $H_1 = 600$ nm, $W_0 = 840$ nm, $W_1 = 1190$ nm, $W_{slot\_left} = 90$ nm, $W_{slot\_right} = 84$ nm). The dispersion curves of the corresponding modes in the waveguide without slots are also plotted in (b) for comparison.

quasi-TM modes. The calculated effective indices (indicated by n_{eff}) of them are shown in Fig. 2(a). According to

$$D = -\left(\frac{\lambda}{c}\right) \cdot \left(\frac{\partial^2 n_{eff}}{\partial \lambda^2}\right). \tag{1}$$

Their dispersion curves are calculated and shown in Fig. 2(b), where c is the light speed and λ is the wavelength in vacuum, respectively. The dispersion curves of quasi TE/TM modes in the reverse ridge waveguide without the two slots are also calculated with the same parameters and shown in Fig. 2(b) for comparison. It can be seen that the dispersion curves of the quasi-TM modes in the waveguide with slots is similar to that of the waveguide without slots. They show two ZDWs in the near-infrared band. The dispersion slopes around these ZDWs are relatively high, leading to narrow near-zero dispersion bands. On the other hand, the dispersion profiles of the quasi-TE modes in two waveguides are quite different. The dispersion of quasi-TE mode in the waveguide without slots rises monotonously as the wavelength increases, resulting in only one ZDW. By introducing two slots into the waveguide, the dispersion of the quasi-TE mode in the proposed waveguide is highly reduced at the region of long wavelength. The dispersion curve shows a flat profile with three ZDWs at 1895 nm, 2575 nm and 3105 nm, respectively. An ultra-broad band of near-zero dispersion (from 1770 nm to 3140 nm with a bandwidth of 1370 nm) is realized. Meanwhile the dispersion is confined between -26 ps/(nm $\cdot$ km) and $+27$ ps/(nm $\cdot$ km) in this band.

The difference between the quasi-TE mode dispersion profiles in the two waveguides is due to the dispersion tailoring effect introduced by the two slots. To show it more clearly, the electric field distributions of the quasi-TE mode at different wavelengths in the proposed waveguide with slots (without slots) are calculated and shown in Fig. 3(a) and (b). It can be seen that, in the waveguide without slots, the electric field concentrates in the waveguide core at all the wavelengths. However, in the proposed waveguide structure, the electric field is concentrated in the

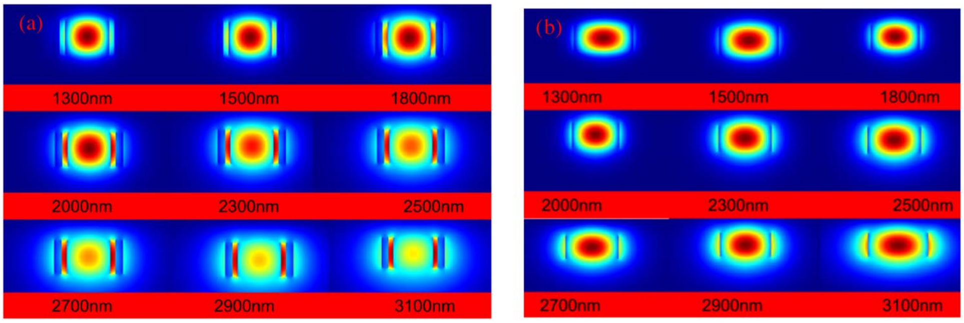

Fig. 3. Quasi-TE mode evolution of the waveguide (a) with slots and (b) without slots for various wavelengths.

waveguide core at short wavelengths. As the wavelength increases, more and more electric field distributes in the slots. At wavelengths longer than 2500 nm, the electric field is mainly distributed in the two slots. This transition process of the electric field distribution introduces a large negative waveguide dispersion at the long-wavelength region, which provides an additional tailoring effect on the dispersion profile of the quasi-TE mode.

The proposed waveguide has the potential for developing nonlinear photonic devices. On one hand, the third order nonlinearity of As_2S_3 glass is high, with a nonlinear Kerr index n_2 of 2.92×10^{-18} m^2/W at 1.55 μm. On the other hand, the index of As_2S_3 is as high as 2.4–2.5 in the near-infrared band. Hence, the interface between As_2S_3 and SiO_2 provides a good light confinement for realizing a small electric field area. The effective area of the quasi-TE mode can be calculated by [9], [18], [29]

$$A_{\rm eff} = \frac{\left|\int (\mathbf{e} \times \mathbf{h}^*) \cdot \hat{z} dA\right|^2}{\left|\int (\mathbf{e} \times \mathbf{h}^*) \cdot \hat{z}\right|^2 dA} \tag{2}$$

where **e** and **h** are the electric field and magnetic field distributions, respectively. The blue curve in Fig. 4 shows that the calculated effective area of the proposed waveguide with optimized parameters increases as the increase of wavelength, and the areas at all the wavelength are smaller than 1.7 μm^2. We also calculated the nonlinear coefficient of the fundamental quasi-TE mode at different wavelengths by

$$\gamma = \left(\frac{2\pi}{\lambda}\right) \frac{\int n_2 [(\mathbf{e} \times \mathbf{h}^*) \cdot \hat{z}]^2 dA}{\left[\int (\mathbf{e} \times \mathbf{h}^*) \cdot \hat{z} dA\right]^2}. \tag{3}$$

The result is shown as the black curve in Fig. 4. It can be seen that the nonlinear coefficient of the quasi-TE mode reduces as the electric field extends with the increasing of wavelength. At the telecom band, the nonlinear coefficient is about 30/W/m, which is about 1.5×10^4 higher than that of the single-mode silica fiber.

3. Dispersion Tailoring by the Structure Parameter Adjustment

The analysis in Section 2 shows that the dispersion profile of the quasi-TE mode in the proposed waveguide is the combination of the original dispersion of the same mode in a waveguide without the slots and the large negative dispersion introduced by the transition process, which provides additional freedom to tailor the dispersion profile. Fig. 5 shows the calculated dispersion of the fundamental quasi-TE mode when one of the structure parameters varies with others, keeping the same as the optimized parameters used in Fig. 2.

Fig. 5(a) is the calculated dispersion of the proposed waveguide with different waveguide height (H_1). It can be seen that the shapes of the dispersions with different height are quite similar although the dispersion value collectively increases with the increase of H_1 at a rate of 2.3 ps/nm/km

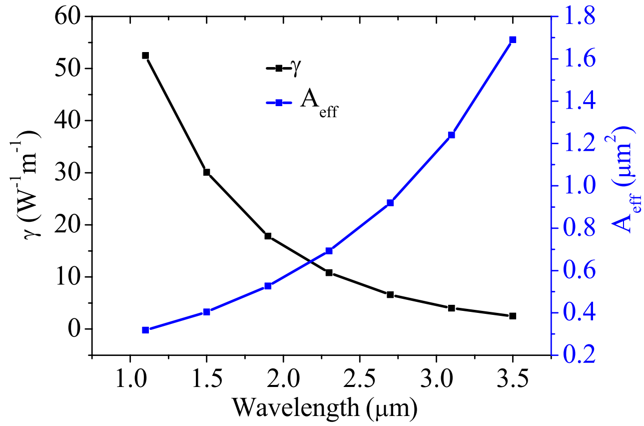

Fig. 4. Effective areas (blue line) and nonlinear coefficient (black line) of the quasi-TE mode in the proposed waveguide with optimized parameters.

per nanometer. This variation is mainly due to the impact of varying H_1 on the original dispersion profile, since H_1 is also a structure parameter of the waveguide without the slots.

Similar effects can be found when adjusting the width of the slots. Fig. 5(b) and (c) shows the calculation results with different widths of the left slot (W_{slot_left}) and the right slot (W_{slot_right}), respectively. It can be seen that, the variation of slot width does not change the shape of the dispersion either. The dispersion value collectively decreases with the increase of slot width at a rate of 2.5 ps/nm/km per nanometer. Rather than the original dispersion, this dispersion variation is introduced by the transition process when varying slot widths. Larger negative dispersion would be introduced by the slots with larger widths.

On the other hand, the variation of waveguide width leads to more complex impact on the dispersion profile. Fig. 5(d) shows the calculation results with different intervals (W_0) between the two slots. It can be seen that the dispersion curve at long-wavelength region nearly remains the same while the dispersion value increases as the increase of waveguide width at short-wavelength region. Therefore, the dispersion slop between the maximum and minimum of the dispersion curve is enhanced with the increasing W_0. It can be seen that the variation of W_0 does not impact the waveguide without the slots, hence the original dispersion profile is unchanged. On the other hand, Fig. 3(b) shows that in the waveguide without the slots, the modal distribution is more concentrating at a shorter wavelength. It can be expected that the transition process would appear at shorter wavelength under a smaller W_0, leading to a lower dispersion at short wavelength region.

Fig. 5(e) shows the calculated dispersion with different waveguide widths (W_1). It can be seen that the maximum of the dispersion curve reduces when W_1 increases. At the same time, the minimum of the dispersion curve increases with the increasing W_1. This indicates that a smaller dispersion slope between the maximum and the minimum of the dispersion can be obtained with larger W_1. On one hand, the variation of W_1 changes the waveguide without the slots leading to a variation of the original dispersion profile. On the other hand, it also impacts the wavelength at which the transition process appears, leading to the variation of the introduced negative dispersion. The result shown in Fig. 5(e) is the combination of these two effects.

The calculation results in Fig. 5 show that the proposed waveguide provides rich freedom to tailor its dispersion profile.

4. Analysis on the Phase Mismatching of the Degenerate Four Wave Mixing Process in the Proposed Waveguide

The ultra-broadband flat and low dispersion property of this waveguide is preferred in many nonlinear optical applications. A typical application is the degenerate four wave mixing (FWM). In this process, the pump light and idler (or signal) light travel in the waveguide and generate the

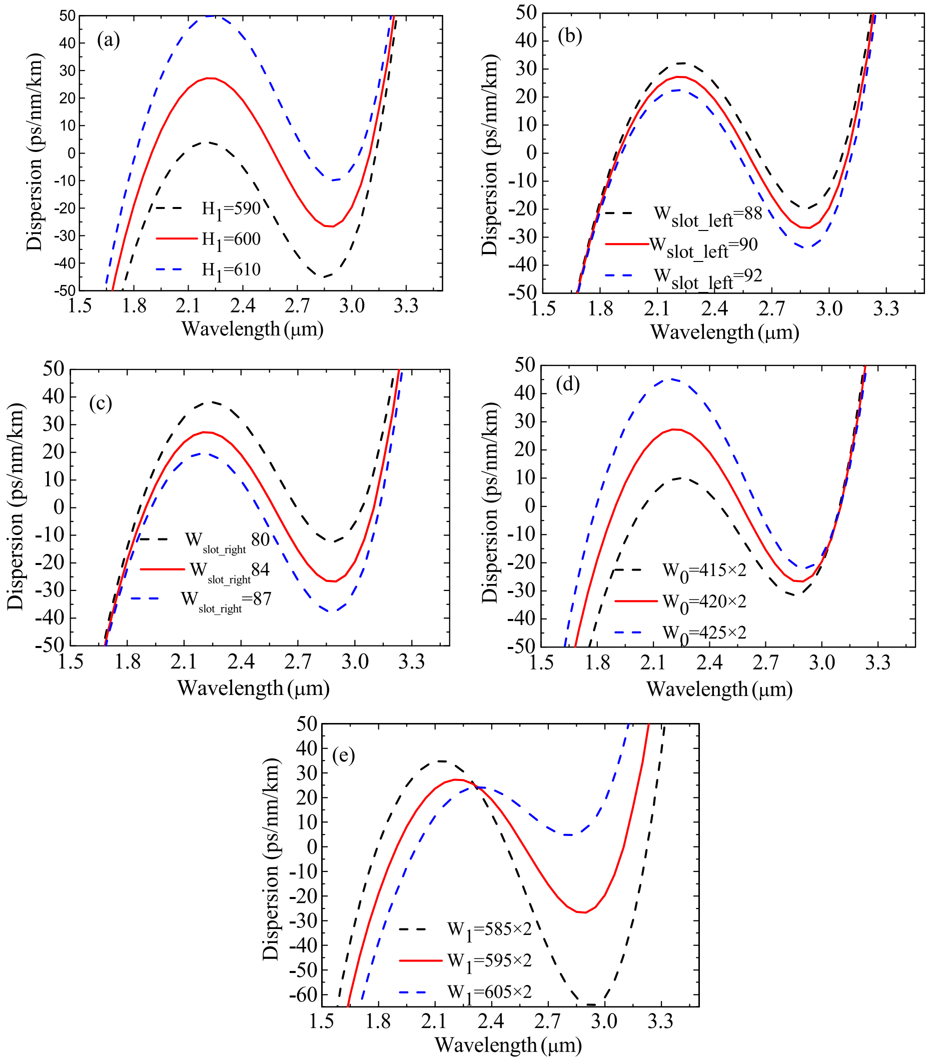

Fig. 5. Dispersion tailoring effects with different structure parameters in the proposed waveguide. (a) Ridge height (H_1). (b) Widths of the left slot (W_{slot_left}). (c) Width of the right slot (W_{slot_right}). (d) Interval between the two slots (W_0). (e) Width of the waveguide (W_1).

signal (or idler) light due to the third-order nonlinearity. The frequencies of pump light ω_p, idler light ω_i and signal light ω_s satisfy $2\omega_p = \omega_i + \omega_s$, indicating the energy conservation in this process. The efficiency of the degenerate FWM process is determined by the phase mismatching $\Delta k = \Delta\beta + 2(\gamma_s + \gamma_i - \gamma_p)P_p$. In this equation, $\Delta\beta = \beta_s + \beta_i - 2\beta_p$ is the linear phase mismatching, where β_p, β_i and β_s are the phase coefficients of pump light, idler light and signal light, respectively. The term $2(\gamma_s + \gamma_i - \gamma_p)P_p$ is the nonlinear phase mismatching, where γ_p, γ_i and γ_s are the nonlinear coefficients of pump light, idler light and signal light, respectively, and P_p is the power of the pump light. The degenerate FWM processes can effectively occur only if Δk is close to zero.

We calculated the linear phase mismatching $\Delta\beta$ as shown in Fig. 6(a), in which the propagating modes of the proposed waveguide at the wavelength of the pump light, idler light and signal light are all in the fundamental quasi-TE modes. The two axis in Fig. 6(a) are pump wavelength λ_p and the wavelength difference between the pump light and the signal (idler) light $\Delta_\lambda = \lambda_s - \lambda_p$ ($\Delta_\lambda = \lambda_p - \lambda_i$), respectively. The calculated linear phase mismatching is indicated by the color in the figure. It can be seen that thanks to the large wavelength region of flat and

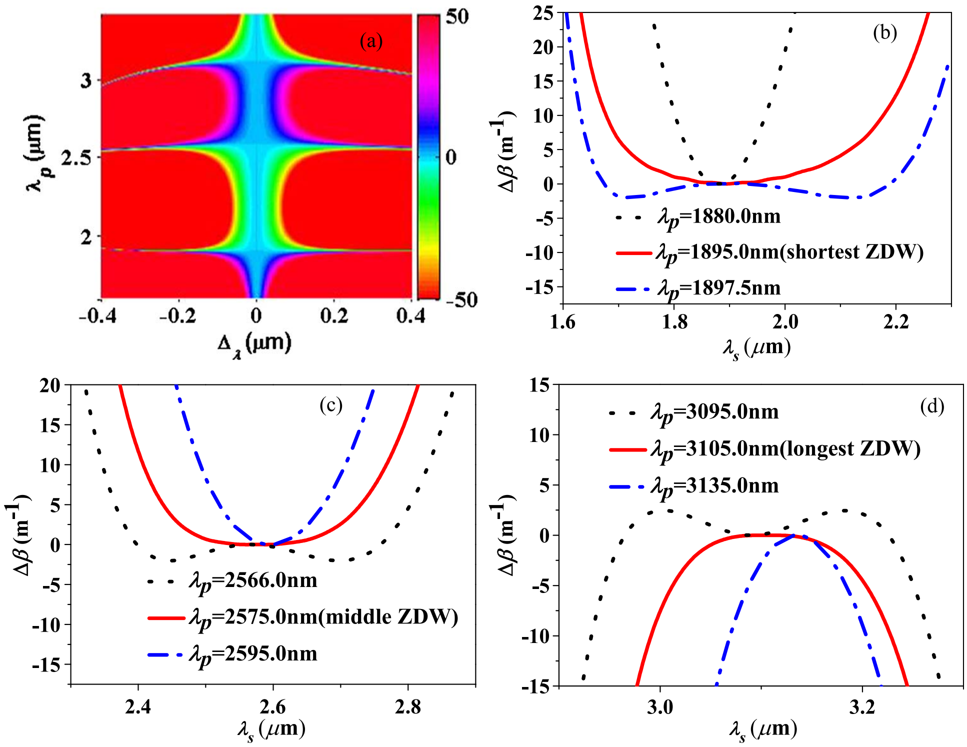

Fig. 6. Calculation results of linear phase mismatching of the degenerate FWM process in the proposed waveguide. (a) Linear phase mismatching $\Delta\beta$ under different pump wavelength and signal-pump wavelength difference Δ_λ. (b) Linear phase mismatching $\Delta\beta$ under different signal (idler) wavelengths when λ_p is set near the shortest ZDW. (c) Linear phase mismatching $\Delta\beta$ under different signal (idler) wavelengths when λ_p is set near the middle ZDW. (d) Linear phase mismatching $\Delta\beta$ under different signal (idler) wavelengths when λ_p is set near the longest ZDW.

near-zero dispersion, the linear phase mismatching $\Delta\beta$ keeps low in a broad range of Δ_λ when pump wavelengths λ_p are located near all the three ZDWs, as shown in Fig. 2(b). Fig. 6(b) shows the result when the pump wavelength λ_p locates near the shortest ZDW (1895.0 nm). When λ_p is exactly 1895.0 nm, the curve of $\Delta\beta$ looks like an upward parabola with a zero point at $\Delta_\lambda = 0$. $\Delta\beta$ is close to zero in a wide band near $\Delta_\lambda = 0$. When λ_p decreases, e.g., to 1880.0 nm, the parabola-like curve shrinks, leading to a smaller near-zero band of $\Delta\beta$. On the other hand, when λ_p increases, e.g., to 1897.5 nm, two regions with negative $\Delta\beta$ appear at two sides, which would be deeper and wider if λ_p further increases. Fig. 6(c) shows the calculation results when pump wavelength locates near the middle ZDW (2575.0 nm). It can be seen that the curve of $\Delta\beta$ changes from an upward parabola to a curve with two negative dips at two sides as the pump wavelength λ_p decreases from 2595.0 nm to 2566.0 nm. Fig. 6(d) shows the calculation results when pump wavelength locates near the longest ZDW (3105.0 nm). When λ_p is exactly the longest ZDW, the curve of $\Delta\beta$ is a downward parabola with a zero point at $\Delta_\lambda = 0$. However, the downward parabola would shrink if the pump wavelength λ_p increases, e.g., to 3135.0 nm. If the pump wavelength λ_p decreases, two positive peaks appear at two sides as the black dotted line shown in Fig. 6(d).

The small negative linear mismatching is preferred for the degenerate FWM process, since the linear mismatching can be compensated by the nonlinear mismatching term at proper pump level. Hence, broadband degenerate FWM could be realized if the wavelength of the pump light is a little longer than the shortest ZDW or a little shorter than the middle ZDW. Besides, if the wavelength of the pump light is a little shorter than the longest ZDW, the degenerate FWM process with large span between the signal and idler wavelength would be expected.

5. Conclusion

In this paper, we proposed a reverse ridge/slot As_2S_3 waveguide with two vertical SiO_2 slots, which could be fabricated without the photolithography, lift-off process, or various etching processes on the As_2S_3 layer. It can support a fundamental quasi-TE mode with an ultra-flat dispersion profile with three ZDWs. In this band, its dispersion is confined between -26 and $+27$ ps/nm/km over a band of 1370 nm (from 1770 nm to 3140 nm). Dispersion design can be realized by tuning structural parameters of the proposed waveguide. Especially, the mode transition process introduced by the two slots provides additional tailoring effects on the waveguide dispersion, which leads to its ultra-flat and near-zero dispersion over a wide bandwidth. The proposed waveguide also has a high $\chi^{(3)}$ nonlinearity, which is demonstrated by the effective area and the nonlinear coefficient of its quasi-TE mode. The properties of high nonlinearity and a large wavelength region of flat and near-zero dispersion are preferred in many nonlinear applications. Since the waveguide has three ZDWs and two of them are at mid-infrared band, it has great potential in developing mid-infrared nonlinear optical devices. To show its potential applications, the phase mismatching of the degenerate FWM process in this waveguide are analyzed, showing that the waveguide can support broadband FWM process in near-infrared and middle-infrared regions.

References

[1] M.-L. Anne *et al.*, “Chalcogenide glass optical waveguides for infrared biosensing,” *Sensors*, vol. 9, no. 9, pp. 7398–7411, Sep. 2009.
[2] J. Charrier *et al.*, “Evanescent wave optical micro-sensor based on chalcogenide glass,” *Sens. Actuators B, Chem.*, vol. 173, pp. 468–476, Oct. 2012.
[3] D. Conteduca, F. Dell'Olio, C. Ciminelli, and M. N. Armenise, “New miniaturized exhaled nitric oxide sensor based on a high Q/V mid-infrared 1D photonic crystal cavity,” *Appl. Opt.*, vol. 54, no. 9, pp. 2208–2217, Mar. 2015.
[4] Y. Zou *et al.*, “High-performance, high-index-contrast chalcogenide glass photonics on silicon and unconventional non-planar substrates,” *Adv. Opt. Mater.*, vol. 2, no. 5, pp. 478–486, May 2014.
[5] R. Won, “On-chip signal processing,” *Nat. Photon.*, vol. 5, no. 12, p. 725, Dec. 2011.
[6] L. Li *et al.*, “Integrated flexible chalcogenide glass photonic devices,” *Nat. Photon.*, vol. 8, no. 8, pp. 643–649, Aug. 2014.
[7] M. R. Lamont, B. Luther-Davies, D.-Y. Choi, S. Madden, and B. J. Eggleton, “Supercontinuum generation in dispersion engineered highly nonlinear $(\gamma = 10/\mathrm{W/m})$ As2S3 chalcogenide planar waveguide,” *Opt. Express*, vol. 16, no. 19, pp. 14 938–14 944, 2008.
[8] F. De Leonardis and V. M. N. Passaro, “Dispersion engineered silicon nanocrystal slot waveguides for soliton ultrafast optical processing,” *Adv. Optoelectron.*, vol. 2011, pp. 1–9, 2011.
[9] L. Zhang *et al.*, “Silicon waveguide with four zero-dispersion wavelengths and its application in on-chip octave-spanning supercontinuum generation,” *Opt. Express*, vol. 20, no. 2, pp. 1685–1690, 2012.
[10] L. Zhang *et al.*, “On-chip octave-spanning supercontinuum in nanostructured silicon waveguides using ultralow pulse energy,” *IEEE J. Sel. Top. Quantum Electron.*, vol. 18, no. 6, pp. 1799–1806, Nov./Dec. 2012.
[11] S. Gao, Z. Li, E.-K. Tien, S. He, and O. Boyraz, “Performance evaluation of nondegenerate wavelength conversion in a silicon nanowire waveguide,” *J. Lightw. Technol.*, vol. 28, no. 21, pp. 3079–3085, Nov. 2010.
[12] Q. Liu, S. Gao, Z. Li, Y. Xie, and S. He, “Dispersion engineering of a silicon-nanocrystal-based slot waveguide for broadband wavelength conversion,” *Appl. Opt.*, vol. 50, no. 9, pp. 1260–1265, Mar. 2011.
[13] P. Del'Haye, O. Arcizet, M. L. Gorodetsky, R. Holzwarth, and T. J. Kippenberg, “Frequency comb assisted diode laser spectroscopy for measurement of microcavity dispersion,” *Nat. Photon.*, vol. 3, no. 9, pp. 529–533, 2009.
[14] Y. Okawachi *et al.*, “Octave-spanning frequency comb generation in a silicon nitride chip,” *Opt. Lett.*, vol. 36, no. 17, pp. 3398–3400, 2011.
[15] M. J. Collins *et al.*, “Low Raman-noise correlated photon-pair generation in a dispersion-engineered chalcogenide As_2S_3 planar waveguide,” *Opt. Lett.*, vol. 37, no. 16, pp. 3393–3395, Aug. 2012.
[16] M. R. Lamont, C. M. de Sterke, and B. J. Eggleton, “Dispersion engineering of highly nonlinear As2S3 waveguides for parametric gain and wavelength conversion,” *Opt. Exp.*, vol. 15, no. 15, pp. 9458–9463, 2007.
[17] J. He *et al.*, “Effect of low-Raman window position on correlated photon-pair generation in a chalcogenide Ge11.5As24Se64.5 nanowire,” *J. Appl. Phys.*, vol. 112, no. 12, 2012, Art. ID. 123101.
[18] Z. Jafari and F. Emami, “Strip/slot hybrid arsenic tri-sulfide waveguide with ultra-flat and low dispersion profile over an ultra-wide bandwidth,” *Opt. Lett.*, vol. 38, no. 16, pp. 3082–3085, Aug. 2013.
[19] L. Zhang, Y. Yue, R. G. Beausoleil, and A. E. Willner, “Flattened dispersion in silicon slot waveguides,” *Opt. Exp.*, vol. 18, no. 19, pp. 20 529–20 534, Sep. 2010.
[20] M. Zhu *et al.*, “Ultrabroadband flat dispersion tailoring of dual-slot silicon waveguides,” *Opt. Exp.*, vol. 20, no. 14, pp. 15 899–15 907, Jul. 2012.
[21] L. Zhang *et al.*, “Flat and low dispersion in highly nonlinear slot waveguides,” *Opt. Exp.*, vol. 18, no. 12, pp. 13 187–13 193, Jun. 2010.

[22] D.-Y. Choi *et al.*, "A protective layer on As2S3 film for photo-resist patterning," *J. Non-Cryst. Solids*, vol. 354, no. 47–51, pp. 5253–5254, Dec. 2008.
[23] D.-Y. Choi *et al.*, "Submicrometer-thick low-loss as S planar waveguides for nonlinear optical devices," *IEEE Photon. Technol. Lett.*, vol. 22, no. 7, pp. 495–497, Apr. 2010.
[24] T. B. Pittman, B. C. Jacobs, and J. D. Franson, "Heralding single photons from pulsed parametric down-conversion," *Opt. Commun.*, vol. 246, no. 4–6, pp. 545–550, Feb. 2005.
[25] X. Gai *et al.*, "Progress in optical waveguides fabricated from chalcogenide glasses," *Opt. Exp.*, vol. 18, no. 25, pp. 26 635–26 646, 2010.
[26] D.-Y. Choi, S. Maden, A. Rode, R. Wang, and B. Luther-Davies, "Plasma etching of As2S3 films for optical waveguides," *J. Non-Cryst. Solids*, vol. 354, no. 27, pp. 3179–3183, Jun. 2008.
[27] Y. Zou *et al.*, "Solution processing and resist-free nanoimprint fabrication of thin film chalcogenide glass devices: Inorganic–organic hybrid photonic integration," *Adv. Opt. Mater.*, vol. 2, no. 8, pp. 759–764, 2014.
[28] Y. Zha, P. T. Lin, L. Kimerling, A. Agarwal, and C. B. Arnold, "Inverted-rib chalcogenide waveguides by solution process," *ACS Photon.*, vol. 1, no. 3, pp. 153–157, 2014.
[29] S. V. Afshar and T. M. Monro, "A full vectorial model for pulse propagation in emerging waveguides with subwavelength structures Part I: Kerr nonlinearity" *Opt. Exp.*, vol. 17, no. 4, pp. 2298–2315, 2009.